Distinct behavioural and network correlates of two interneuron types in prefrontal cortex

D. Kvitsiani[1],[*], **S. Ranade**[1],[*], **B. Hangya**[1], **H. Taniguchi**[1], **JZ. Huang**[1], and **A. Kepecs**[1]

[1]Cold Spring Harbor Laboratory, 1 Bungtown Road, Cold Spring Harbor, NY, 11724

Abstract

Neurons in prefrontal cortex exhibit diverse behavioural correlates[1–4], an observation that has been attributed to cell-type diversity. To link identified neuron types with network and behavioural functions, we recorded from the two largest genetically-defined inhibitory interneuron classes, the perisomatically-targeting parvalbumin (*Pv*) and the dendritically-targeting somatostatin (*Som*) neurons[5–8] in anterior cingulate cortex (ACC) of mice performing a reward foraging task. Here we show that *Pv* and a subtype of *Som* neurons form functionally homogeneous populations showing a double dissociation between both their inhibitory impact and behavioural correlates. Out of a number of events pertaining to behaviour, a subtype of *Som* neurons selectively responded at reward approach, while *Pv* neurons responded at reward leaving encoding preceding stay duration. These behavioural correlates of *Pv* and *Som* neurons defined a behavioural epoch and a decision variable important for foraging (whether to stay or to leave), a crucial function attributed to ACC[9–11]. Furthermore, *Pv* neurons could fire in millisecond synchrony exerting fast and powerful inhibition on principal cell firing, while the inhibitory impact of *Som* neurons on firing output was weak and more variable, consistent with the idea that they respectively control the outputs of and inputs to principal neurons[12–16]. These results suggest a connection between the circuit-level function of different interneuron-types in regulating the flow of information, and the behavioural functions served by the cortical circuits. Moreover these observations bolster the hope that functional response diversity during behaviour can in part be explained by cell-type diversity.

To investigate whether distinct interneuron types can encode specific behavioral variables we recorded the activity of inhibitory neurons expressing parvalbumin (*Pv*) and somatostatin (*Som*) markers (Supplementary Fig. 1a). *Pv* basket cells are thought to control the spiking output of pyramidal neurons[12,14] while a majority of *Som* interneurons, known as

'Martinotti cells' (Supplementary Fig. 1c and d), target distal dendrites, gating the inputs arriving onto pyramidal cells[13,15,17–20]. To target these interneuron types for recordings, we used *Pv-Cr*e and *Som-Cr*e[21,22] driver mouse lines in combination with AAV viruses to deliver channelrhodopsin (ChR2)[23], rendering neurons light sensitive (Supplementary Fig. 1a and b). Miniature microdrives housing 6 movable tetrodes and an optical fiber were implanted in deep layers of ACC (Fig. 1b, Supplementary Fig. 1e-g). We recorded well-isolated single units (n=1339 from 6 *Pv-Cr*e and 6 *Som- Cr*e mice) and delivered brief pulses (1 ms) of blue light to elicit short-latency action potentials in ChR2-expressing neurons that served as a physiologic tag[24] (Fig. 1a, c). To identify directly light-activated units we developed an optical-tagging test based on a statistical measure that yields a *P*-value testing whether light-activation induced significant changes in spike timing (Fig. 1d and Supplementary Fig. 2, see Methods). Significantly activated units ($P < 0.01$) showed similar spontaneous and light evoked waveforms (correlation coefficient, $r > 0.85$, Fig. 1a, Supplementary Fig. 2c), low-latency light-induced response (< 4 ms), and low first-spike jitter (Supplementary Fig. 2d), signatures of direct light-activation.

Extracellularly recorded units are traditionally classified based on spike width and firing rate, with narrow-spiking and fast-firing neurons categorized putatively as *Pv* interneurons[1,25]. Indeed, most identified *Pv* neurons were narrow-spiking with high firing rates (219±10 μs, 31±3 Hz, n=23, Fig. 1e) while the spike-width distribution for *Som* units was bimodal (Fig. 1e, bottom panel): a third of neurons had narrow spikes ("NS", <270 μs) and high firing rates (212±7 μs, 16±4 Hz, n=13), while the rest showed markedly wider spike waveforms and lower firing rates ("WS", 327±7 μs, 4±1 Hz, n=22).

Having identified *Pv* and *Som* interneurons, we first examined their impact on local circuit activity. Synchronous photostimulation of ChR2-expressing *Pv* or *Som* neurons had markedly different network effects, with *Pv* neurons imposing brief uniform inhibition on nearby neurons[26], and *Som* neurons exerting longer and more variable inhibition (Fig. 2a and b, Supplementary Fig. 3a and b). These differences cannot be accounted for by systematic differences in the number of photo-activated neurons (Supplementary Fig. 4) and indicate that *Som* and *Pv* neurons exert distinct inhibitory footprints on network activity.

Optogenetic identification of many individual interneurons, in combination with simultaneous recording from a large number of their neighbours, allowed us to investigate the physiological impact of different inhibitory subtypes during behavioural epochs without light stimulation. To identify possible functional connectivity between neurons, we computed cross-correlograms (CCGs): counts of spike co-occurrences in the putative pre- and postsynaptic neuron pairs at different time lags[27] (Fig. 2c). Significant short-latency interactions were rare among pairs of unidentified ACC neurons (3.2% inhibitory, 5.2% excitatory, 1.3% both, out of 2945 pairs, bootstrap test with $P < 0.001$ used for all CCG significance testing). Remarkably, 5/7 pairs of *Pv* neurons showed interactions with 3/7 firing in millisecond zero-lag synchrony, and 4/7 inhibited each other (trough at 2.25±0.5 ms, Fig. 2c, Supplementary Fig. 5a and c). *Pv* neurons also showed a high prevalence of short-timescale correlations with unidentified neurons (38/152 pairs, $P < 0.001$, Fig. 2c, Supplementary Fig. 5c), often with detectible inhibition (trough at 2.39±1.3 ms, 18/152

pairs, $P < 0.001$). These results demonstrate that the *Pv* population is capable of millisecond synchronization with fast and precise inhibitory impact on local neural activity.

In contrast to *Pv* pairs, we found no short-timescale correlations between *Som* pairs (0/11, 7 WS-WS and 4 NS-WS pairs, Fig. 2c, Supplementary Fig. 5b), and the influence of both NS-*Som* and WS-*Som* on unidentified neurons was sparser and more diverse (15/169 pairs, inhibitory in 2/169, $P < 0.001$, Fig. 2c, Supplementary Fig. 5c, —note that the weak observable impact of *Som* neurons on the firing output of their neighbours could be due to dendritic inhibition generating input suppression, which is expected to be more difficult to detect using a cross-correlation approach). Thus, *Pv* and *Som* interneurons form distinct inhibitory networks: a fast, synchronous *Pv* network generating strong, transient inhibition and an asynchronous *Som* network with weaker impact on firing output.

Next we explored whether these cell-type differences in network functions are also reflected in specific behavioural correlates. To engage neural ensembles in ACC we employed a task that incorporated cue-based prediction, temporal control of actions and reward foraging decisions (Fig. 3a). Mice were trained to run back and forth on a linear track between two platforms to collect water rewards; entering one platform ("trigger-zone") enabled reward availability at the other ("reward-zone"). As mice ran back to the reward-zone platform, reward size was cued by an auditory signal. This task mimics the self-paced timing of foraging behaviours and exploits the natural tendency of mice to trade staying in a rewarded, safe area with running on an elevated open track to enable future reward collection. Behavioural performance was sensitive to anticipated reward outcomes since on a subset (15%) of trials in which the cue and reward were omitted, mice slowed their speed during reward zone approach (Fig. 3b).

We examined the responses of a population of 1034 neurons (from 4 *Pv*-Cre and 6 *Som*-Cre mice) in the task. Neurons responded at several behavioural events and modulated their firing by different behavioural variables. For instance, as expected of neurons in ACC[3,9,11] we found single neuron correlates of reward prediction, staying time, and reward outcome and size (Supplementary Fig. 6a). The firing of many individual neurons was selective for single as well as combinations of task variables without any apparent clustering of response properties (Supplementary Fig. 6b–e). Therefore we used an unbiased approach to determine firing rate modulation patterns for *Pv* and *Som* neurons, which focused our analysis on two behaviourally relevant events, reward approach and leaving (see Methods, Supplementary Fig. 6f), Similar to the example neuron (Fig. 3c), most recorded *Pv* neurons (11/14) phasically increased their firing as mice left the reward zone (Fig. 3d, Supplementary Fig. 7c and 8a, b). To test the homogeneity and specificity of these event-related response profiles we used a resampling approach and compared *Pv* interneurons to the unidentified population (see Methods). We found that the temporal response profiles of *Pv*s were homogeneous ($P < 0.01$, bootstrap test) and distinct ($P < 0.001$) compared to randomly selected groups of neurons (see also Supplementary Fig. 9d). Moreover, knowledge of *Pv* identity carried approximately twice the information about the time course of responses than knowledge that a neuron is narrow-spiking, despite the fact that *Pv* neurons tend to be narrow-spiking ($P < 0.05$, Supplementary Fig. 7b).

The firing of many *Som* neurons was strongly suppressed at the time of reward zone entry (13/21, suppression index < 0, $P < 0.01$, permutation test), like the example neuron (Fig. 3e). Similarly, most NS-*Som* neurons were suppressed upon entry into the reward zone (9/10, Fig. 3f, lower panel, Supplementary Fig. 8a, b). In contrast, WS-*Som* neurons were activated at different moments in time, around the entry into the reward zone (Fig. 3f, upper panel). These profiles were different from both the *Pv* and the unidentified population (Supplementary fig. 7a, d). In concert with their local-circuit effects described above, these observations support the idea that *Som* neurons comprise at least two functional subtypes[18,19,28], a narrow-spiking, more homogeneously responding population and a wide-spiking population with heterogeneous response profiles.

Next we examined whether these cell-type-specific differences in behavioural correlates are also reflected in their synaptic partners. We characterized the responses of unidentified wide-spiking (putative pyramidal, or pPyr) neurons that showed significant inhibitory cross-correlations with identified interneurons (CC-partners, e.g. Fig. 2c, lower panels, inset). Interestingly, *Pv*→pPyr and *Som*→pPyr pairs, which both showed negative cross-correlations on the time scale of milliseconds, exhibited opposing behavioural response-dynamics on the time scale of seconds (Fig. 3g, h). This was not observed for simultaneously recorded neurons without significant short-term interactions with *Pv* or *Som* neurons (Fig. 3g, h). These results reveal that functional connectivity, as identified by millisecond cross-correlations indicative of anatomical connections, also predicts post-synaptic neural responses on the time scale of seconds as relevant for behaviour.

Finally, we sought to better understand the behavioural functions of the *Pv* population. We wondered whether the phasic recruitment of *Pv*s is related to a specific movement or reflects a more abstract behavioural variable (Supplementary Fig. 9c). Specifically, ACC has been implicated in foraging decisions[9,11] — whether to stay or to leave. Therefore, we trained mice on a task version in which they were rewarded at a water port after a fixed 1s delay from entry. In this task variant, the motor program required for the leaving action was a backward movement (Fig. 4a, cartoon), distinct from the forward movement corresponding to reward-zone exit in the original task version. In addition, this enabled more precise measurements of behavioural timing. Mice stayed inside the port for varying durations (2.0±2.2 s) to consume water reward then exited to initiate the next trial. We found that *Pv* neurons responded with a large phasic firing rate elevation around the time of exit from the reward port (Fig. 4d, Supplementary Fig. 8a, b; 11/12 neurons with activation index > 0, $P < 0.05$, permutation test). Because mice could freely exit at any time, we wondered if the activity of these neurons was modulated by the duration of their stay inside the reward port. Indeed, we observed that the firing rate of *Pv* neurons parametrically increased with longer staying times on a trial-by-trial basis (Fig. 4a–d). A similar representation of stay duration has been found in monkey ACC during a foraging task, which was shown to signal the negative value of staying or equivalently the likelihood of leaving during foraging decisions[9]. This suggests that the graded phasic response of *Pv* neurons in ACC is related to a foraging decision, to leave the reward consumption area and initiate a new run.

Our findings demonstrate that two major classes of interneurons not only provide distinct modes of inhibition but also display unique behavioural correlates, with temporal and

functional specificity comparable to principal neurons. Out of the many behavioural events in the task, the homogeneous responses of *Pv* and NS-*Som* interneurons bracketed a defined epoch: from reward approach to leaving, and represented a specific behavioural variable, staying time at the reward-zone, critical for foraging decisions, a central function attributed to ACC[9,10]. How can this temporal and behavioural specificity be understood in the context of our current knowledge of interneurons? First, tuning specificity may arise from the dense, convergent local input these interneuron types receive[7,29], enabling them to "summarize" local neural activity, which may be particularly high at the moments when a region is engaged in a task[30]. Second, *Pv* interneurons have been implicated in controlling pyramidal cell output[12,14,16], consistent with the synchronous firing and strong inhibitory coupling we observed. In contrast, *Som* neurons are thought to gate long-range inputs to principal cells[13,15,17,20], and their asynchronous activation and weaker inhibitory impact on firing output is consistent with this role. In our behaviour, input and output regulation might be expected around the foraging decision, consistent with the observed suppression of NS-*Som*s during approach followed by the activation of *Pv*s at reward exit. Taken together, our findings suggest a conceptual model in which these interneuron subtypes specialize in temporally regulating the flow of information in a given cortical circuit during the behavioural events relevant to that area. In summary, these observations bolster the long-held hope that probing identified cell-types will reveal the intrinsic logic of cortical circuits under more natural behavioural settings[5,6].

Methods

Microdrive construction

We designed two microdrive models that enabled concurrent optical stimulation and recording of neuronal activity. The plastic frame for the drives was designed using AutoCAD Inventor (Autodesk, Inc) and 3D printed (Vista Technologies). In one microdrive model (3.5 g) the frame can house up to 10 individually moveable shuttles and is well suited to record and optically activate large population of neurons. Each shuttle has precision holes drilled to attach the tetrode and/or optical ferrule and a miniature screw (0.6 mm OD, 12 mm length) with a pitch of 160 μm. An electronic interface board (EIB32, Neuralynx, Inc.) connects tetrodes to the preamplifier (HS36, Neuralynx, Inc.). The fibre-optic probe for optical stimulation consists of a polyimide coated multimode fibre (60 μm dia., Polymicro Technologies) glued into a fibre-optic ferrule (LC ferrule 80 μm, Precision Fibre Products, Inc.). The ferrule end is polished using standard optical methods for efficient light coupling and the other end is precisely cleaved for insertion into the brain. The other microdrive model can house up to 5 independently adjustable shuttles and weighs 2.2g when loaded with a single shuttle that houses a bundle of 6 tetrodes and an optical fibre (Supplementary Fig. 1e).

Viral injection

Adeno-associated virus (AAV) 2/9 serotype (8×10^2 genome copies per ml, UNC Vector Core Facility) carrying EF1a-DIO-ChR2-EYFP or EF1a-DIO-Arch-EYFP construct[31,32] was injected in 1 month old *Pv*-Cre and *Som*-Cre male mice. Mice were anaesthetized with an intraperitoneal injection of ketamine-xylazine mixture (0.13 mg/g body weight ketamine,

0.01 mg/g xylazine). Exposed skin surfaces were occasionally irrigated with lidocaine. A small craniotomy was made above the left dmPFC (2 mm AP, 0.5 mm ML, from bregma). Virus was injected with a glass micropipette using a Picospritzer (General Valve). 20–60 pulses of 10 ms duration were delivered at 0.2 Hz starting from a depth of 1.9 mm from the brain surface up to 1.2 mm in 100 μm steps, waiting a minimum of 2–3 min per site to allow diffusion of the virus. Animals were allowed to recover for at least 2 weeks for optimal viral expression.

Microdrive implantation

After anaesthesia a ~1 mm diameter hole was drilled through the skull at the site of viral injection. Animals received supplemental dose of anaesthetic at 30–90 minute intervals to maintain depth of anaesthesia. The microdrive was positioned with the help of a stereotaxic arm (David Kopf Instruments) above the craniotomy with protruding tetrodes. The optical fibre and tetrodes were gradually lowered to a depth of 500 μm from brain surface. Two 0.25 mm diameter stainless steel wires (Alpha Wire Company) were stripped at the end and inserted into cerebellum and right parietal lobe to a depth of ~1 mm below dura to serve as reference and ground electrodes respectively. Two miniature watch screws (Micro-Mark) were fixed into the parietal plates as anchors. The microdrive was secured to the skull with UV light curable dental cement (Vitrebond Plus) followed by a layer of black dental acrylic (Lang Dental Manufacturing Co.) Tetrodes and optical fibre were lowered by a further 320 μm before mice recovered from anaesthesia. For post-operative analgesia, ketoprofen (2 mg/kg body weight) was administered intraperitoneally. Mice were allowed to recover for at least a week.

Foraging task: behavioral setup, training

The behavioral setup consists of an elevated linear track (length 45 cm, width 5 cm) that connects two 8x10 cm platforms (termed 'reward-zone' and 'trigger-zone'). Water rewards were delivered at the reward-zone either through a lick tube at the end of the reward zone (Fig. 3a) or a water port designed to precisely monitor timing of port entry and exit (Fig. 4a, inset). Position of the mice on the track was monitored at 30 Hz with a spatial resolution of 2 mm/pixel using a video tracker that tracked 1 red and 1 green LED integrated into the preamplifier on the microdrive (Neuralynx Inc.). The behavioral hardware (valves, light-sensors) and the laser were triggered via a data acquisition board (National Instruments PCI-MIO-16E-1) controlled by custom Matlab programs (Mathworks, Natick, MA). Position was tracked by Cheetah recording software (Neuralynx, Inc). Due to the additional weight of the preamplifier and cable we used a custom-designed commutator and counterbalance assembly to enable mice to run more freely. The counterbalance consists of a 40 cm boom moving freely on air bearings with a spherical socket at the end acting as an air bearing commutator. Precisely controlled and frictionless counterbalancing force was achieved using a pneumatic actuator. The tether was suspended by a hollow ball glued to it that floated inside the socket, and was connected to a slip-ring commutator (PSR-27, Neuralynx Inc.) to release torque accumulated by the tether.

1–3 weeks after surgery mice were trained to run on the track. In the initial phase of training, mice were provided with water whenever they approached either the reward-zone or poked

into the water port. After consuming 20–40 rewards, mice were conditioned to obtain water by running to the opposite end of the platform, the trigger-zone, and running back to collect the reward. Entry into the trigger-zone activated an auditory cue, which signaled availability of water at the reward-zone. Once mice performed about 60 runs we introduced different reward sizes (small: 2–4 μl, large: 6–12 μl) signaled by distinct auditory cues (mixture of high frequency and low frequency tones, 0.1 s duration). Mice also received a reminder auditory cue immediately after exiting the trigger-zone (Fig. 3a). On a small fraction of trials (15%) reward was omitted. Mice performed 60–200 trials per session lasting 1–2 hours. Animals were kept on a water restriction schedule to maintain 85–90% of free-drinking weight.

Neural data collection and optical stimulation

Electrophysiological recordings were performed using a Neuralynx Cheetah 32 system. Electrical signals were split and separately amplified and filtered for local field potentials (LFPs) and single unit activity. The signal was band-pass filtered between 600–6000 Hz and sampled at 32 kHz to record spiking activity, while LFPs were filtered between 0.1–400 Hz and acquired at 3 kHz. We used 6 tetrodes and one optical fibre to record a total of 1339 single units from 12 mice. Of these, 1034 neurons (from 4 *Pv*-Cre and 6 *Som*-Cre mice) were recorded during the foraging task and 305 neurons (from 2 *Pv*-Cre mice) were recorded in the port variant of the same task. We recorded a total of 28 *Pv* cells from ACC in 5 *Pv*-Cre animals (5,5,6,2,10 cells from each animal out of 15,14,19, 24,41, sessions respectively) and 35 cells from 6 *Som*-Cre animals (14,4,2,3,10,2 cells per animal with 29,12,16,17,13,12 sessions respectively). In addition we recorded one *Pv*-Cre animal that gave no tagged neurons. Neurons that had baseline firing rate < 1Hz or showed no activity during perievent periods (window size was specific for each event, see below) were excluded from behavioral analyses.

An optical multimode fibre (55 μm diameter *NA=0.7*, Polymicro Technologies) was coupled via a modified LC-LC type connector to a multimode fibre (126 μm diameter *NA=0.27*, CablesPlus USA), which collected light from a blue laser (473 nm; 20 mW; CrystaLaser). Maximal power at the tip of the fibre ranged from 10% to 30% of power at the light source resulting in 2–6 mW of total output at the fibre tip.

In order to evaluate spatial extent of light on brain tissue we conducted (i) photobleaching experiments to measure the area of a bleached fluorophore and (ii) c-fos staining around the fibre tip. For photobleaching experiments blue light (473 nm, 2–4 mW power) was applied continuously for 1hr while for c-fos induced expression we applied the same light for 1hr in 1ms pulses at 20 Hz. The spread of light in photobleaching experiments was ~1000 μm (dorso-ventral axis) by 500 μm (medio-lateral axis). Maximum c-fos induction occurred within a 0.5 mm^2 area (Supplementary Fig. 4a–c). Since our tetrodes were well within 500 μm from the tip of the optical fibre, light reach is not expected to be a limiting factor for optical tagging.

To avoid photo-electric artifact due to light stimulation[33], we positioned our tetrodes parallel to the fibre and in cases where we saw an artifact, we minimized it by lowering the light intensity. We verified the validity of optical tagging by comparing the average peak-aligned

spontaneous waveform with average light evoked waveform using Pearson's correlation coefficient ($r>0.85$).

The light stimulation protocol (15–30 min) for optogenetic tagging was performed at the end of each recording session consisting of 1–2 ms light pulses at 4, 10, 16, 40, and 100 Hz frequencies. The fibre and tetrodes were lowered 20–40 μm every day after each recording session.

Data analysis

All data analysis was carried out using built-in and custom-built software in Matlab (Mathworks, Natick, MA).

Spike sorting—Spikes were manually sorted into clusters (presumptive neurons) off-line based on peak amplitude and waveform energy using MClust software (A.D. Redish). Cluster quality was quantified using *isolation distance*[34] and *L-ratio*[35]. Clusters with *isolation distance < 18 or L-ratio > 0.2* were excluded (*median isolation distance, 29; median L-ratio, 0.033*, see Fig S2a, b). Autocorrelation functions were inspected for all putative cells. In cases where the autocorrelation showed absolute refractory period violations, we improved cluster separation, otherwise, the cluster was excluded.

Detection of light-induced inhibition—To detect light-induced inhibition we first determined the putative suppression period using adaptive smoothing of the PSTH and then evaluated the statistical significance of the firing rate suppression compared to a stimulus-free baseline. First, spike rasters were convolved with a variable kernel Gaussian function to provide a spike density function (SDF) estimate. The kernel width of the Gaussian window was adapted to the local estimate of spiking probability to implement stronger smoothing when information was sparse. Variance was mapped onto spiking probability between 0 (moving average, corresponding to probability of 0) and infinity (Dirac-delta, corresponding to probability of 1). Next, minimal firing was assessed as the minimum of the SDF within 100 ms from light pulse onset. The baseline firing rate was calculated from mean firing probability within a 100 ms window before the start of a pulse train. If the minimal firing after stimulation was lower than 50% of baseline firing rate, then we determined the putative suppression period as the epoch between the half-baseline crossings before and after the minimum. The statistical significance of this suppression was determined by comparing the spike count distribution within this suppression period with an equivalent baseline period using the Mann-Whitney U-test ($P < 0.05$). Note, that we used a 50% baseline minimum to provide sufficient statistical power to the spike rate comparison and to avoid false detection of random fluctuations in firing rate.

Cross-correlation analysis—Cross-correlations between spike trains were calculated using 1 ms bin size and their statistical significance was evaluated using a modified temporal shuffling method. To infer putative monosynaptic interactions from extracellularly recorded neurons it is critical to rule out co-firing arising from slow time-scale covariations, for instance due to common input[39,40] or oscillatory modulations[41]. Under the assumption that spike trains are independent of one another, the shift predictor can be used to establish

the expected level of firing co-occurrence. However, common input or other slow-time scale fluctuations can create trial-to-trial co-variations independent of synaptic interactions. We dealt with the issue of multiple time-scale effects in two ways. First, we used spectral filtering to remove slow time-scale interactions for which shuffle techniques are ill-suited and then used temporal shuffling to establish the expected level of correlations.

First, the full-length cross-correlation function was computed and high-pass filtered at 4 Hz. For the shuffling, we pseudo-randomly selected 5000 instances of 30 ms windows from the filtered cross-correlation function, between 100 ms and 5 s time lags. This is equivalent to calculating the cross-correlation of time-shifted data (sometimes called the shuffling method [42–44]). The cross-correlation function was then low-pass filtered at 4 Hz to calculate the slow trends previously filtered out (see above). This slow modulation was added back to the shuffled cross-correlations in order to obtain estimates of cross-correlation that are not distorted by the filtering procedure. This step is necessary to make the shuffled and the original cross-correlations comparable. Significance limits (set to 0.001 for these analyses) were computed based on the distribution of the shuffled cross-correlations. Statistically significant short-latency suppression after a presynaptic spike is generally taken as evidence for monosynaptic inhibitory connections[45,46] and our results examining identified inhibitory neurons bolster this inference.

For group averages, cross-correlations were standardized by subtracting the mean and dividing by the standard deviation of the shuffled cross-correlograms. Pairwise cross-correlation was performed only on units recorded from different tetrodes to avoid artifactual dips (0 ± 750 µs) in cross-correlogram due to the censored period (spike detection dead time), imposed by spike triggering. For *Pv* and *Som* "CC-partners" (wide spiking neurons with significant inhibitory cross-correlations with *Pv* and *Som* interneurons) we also included units from the same tetrodes. Inhibition onto CC partners was considered significant only when dips in cross-correlogram were significant beyond +1ms for two or more bins. We included spikes collected during behavioral sessions and excluded spikes occurring during the optical tagging epochs.

Identification of putative Pv interneurons for cross-correlation analysis—We identified putative *Pv* neurons based on three criteria: response profile similarity to identified *Pv* neurons, high firing rate (>15 Hz) and narrow spike width (<270 µs). The combination of these 3 features enabled us to identify a distinct cluster of p*Pv*s. Note that our selection algorithm differs from previous studies in that we could make use of the homogeneous firing pattern of identified *Pv* expressing interneurons with respect to behavioural events (Supplementary Fig. 12a). We only selected putative *Pv* interneurons from the second experiment (Fig. 4) incorporating the water port for precise measurement of exit time, that showed the most homogeneity, thus enabling us to confidently isolate putative *Pv* cells. Also note that our aim was not to find all *Pv* neurons, which appeared as false negatives in our dataset due to insufficient ChR2 expression or limited light power but rather to find some cells that resemble identified *Pv* cells enough to conclude with high confidence that they belong to the *Pv* group. We identified 11 putative *Pv* interneurons. Of these neurons, 3 pairs were recorded simultaneously and 2 were recorded along with identified *Pv* cells, yielding 5 new pairs altogether. We found that 4 out of 5 pairs showed significant

short latency interaction in cross-correlograms (3 pairs showed both inhibition and synchrony, 1 pair showed synchrony only) (Supplementary Fig. 12b).

Response modulation index—In order to quantify and compare the selectivity of neural responses to behavioral events, PETHs (±0.5 s window, 50 ms resolution) were calculated for all neurons with reference to each event (reward-zone-exit, reward-zone-entry, trigger-zone-exit, trigger-zone-entry, water-valve-on). Significance limits were assessed by upper and lower 0.005 percentiles of shuffled PETHs. Shuffling was performed with a similar method to cross-correlation analysis, with random shifts between the firing rates and the events ranging from 10 to 30 s, shuffling was performed 2000 times). Response modulation index for each neuron and event was computed as the standard deviation of the PETH. To compute overall selectivity profiles, modulation indices for significantly modulated PETHs was averaged for different neuronal populations (*Pv*, *Som*, Not tagged) for each event (Supplementary Fig. 6f).

Activation and suppression indices—The modulation indices (activation index for reward-zone exit and suppression index for the reward-zone entry events) were both calculated using receiver operating characteristic (ROC) analysis to provide a graded measure and a significance value associated with them[48]. These indices represent scaled version of ROC area (AUC) between two firing rate distributions before and after the event (window size, 0.4 s). We scaled AUC so that it ranges from −1 to 1 with the sign denoting whether a neuron is activated or suppressed.

Modulation index $= 2(ROC_{area} - 0.5)$ and $ROC_{area} = \int_{-\infty}^{\infty} P(f_{before} = f) P(f_{after} < f) df$ where f_{before} and f_{after} refer to the firing rates before and after the relevant event. Statistical significance was evaluated using a permutation test, where trial order was pseudo-randomly shuffled 1000 times to yield a P-value.

Preference index—To compute preference index during various behavioral epochs, trials were divided into two groups according to cue (Cue1 and Cue 2), staying time (shorter and longer than median staying time) and reward size (small and large reward). Firing rates within a fixed peri-event time window (200 ms for cue, 1 s for staying time, and 500 ms for reward preference) were compared using ROC analysis identical to *activation* and *suppression indices*. A significant cue preference index of less than 0 means that the neuron preferentially fires for Cue1 while more than 0 means preference for Cue2, similarly for staying time preference (long = −1, short = 1), and reward preference (small = −1, large = 1).

Staying time modulation of firing rates—We assessed the dependence of firing rate at the reward port on staying time after exit from the reward port on a trial-by-trial basis using robust regression. To determine activation for *Pv* neurons, a window of 0–0.4s was used.

Bootstrap test of homogeneity and firing rate modulation—We performed the following bootstrap tests to compare *Pv* PETHs aligned to reward zone exit to the not tagged population.

Author Manuscript

Author Manuscript

Author Manuscript

Author Manuscript

1. *Test of homogeneity*. The within-group homogeneity of the *Pv* population was computed by averaging pair-wise correlations (Pearson correlation coefficient) of z-scored PETHs aligned to the reward-zone-exit event. This estimate of homogeneity was then tested against the average pair-wise correlation calculated for randomly selected groups of not tagged neurons with the same sample size (1000 bootstrap samples).

2. *Test of firing rate modulation*. The phasic positive modulation of *Pv* neurons was quantified by the average correlation between *Pv* PETHs aligned to reward-zone-exit and a template of event-locked firing rate increase. This template was computed as mean z-scored PETH of all positively modulated not tagged neurons ($P < 0.05$, activation index > 0, *n=107*, permutation test). This estimate of positive firing rate modulation for *Pv* neurons was tested against a bootstrap sample of similar estimates for not tagged neurons in the same manner as for the 'test of homogeneity' (see above).

Supplementary Material

Refer to Web version on PubMed Central for supplementary material.

Acknowledgments

References

1. Constantinidis C, Williams GV, Goldman-Rakic PS. A role for inhibition in shaping the temporal flow of information in prefrontal cortex. Nature Neuroscience. 2002; 5:175–180. [PubMed: 11802172]

2. Machens CK, Romo R, Brody CD. Functional, but not anatomical, separation of "what" and "when" in prefrontal cortex. The Journal of Neuroscience: The Official Journal of the Society for Neuroscience. 2010; 30:350–360. [PubMed: 20053916]

3. Narayanan NS, Laubach M. Top-Down Control of Motor Cortex Ensembles by Dorsomedial Prefrontal Cortex. Neuron. 2006; 52:921–931. [PubMed: 17145511]

4. Wallis JD, Kennerley SW. Heterogeneous reward signals in prefrontal cortex. Current opinion in neurobiology. 2010; 20:191–198. [PubMed: 20303739]

5. Isaacson JS, Scanziani M. How inhibition shapes cortical activity. Neuron. 2011; 72:231–243. [PubMed: 22017986]

6. Klausberger T, et al. Brain-state- and cell-type-specific firing of hippocampal interneurons in vivo. Nature. 2003; 421:844–848. [PubMed: 12594513]

7. Markram H, et al. Interneurons of the neocortical inhibitory system. Nat Rev Neurosci. 2004; 5:793–807. [PubMed: 15378039]

8. Hartwich K, Pollak T, Klausberger T. Distinct firing patterns of identified basket and dendrite-targeting interneurons in the prefrontal cortex during hippocampal theta and local spindle oscillations. J Neurosci. 2009; 29:9563–9574. [PubMed: 19641119]

9. Hayden BY, Pearson JM, Platt ML. Neuronal basis of sequential foraging decisions in a patchy environment. Nature Neuroscience. 2011; 14:933–939. [PubMed: 21642973]

10. Kolling N, Behrens TE, Mars RB, Rushworth MF. Neural mechanisms of foraging. Science. 2012; 336:95–98. [PubMed: 22491854]

11. Quilodran R, Rothe M, Procyk E. Behavioral shifts and action valuation in the anterior cingulate cortex. Neuron. 2008; 57:314–325. [PubMed: 18215627]

12. Atallah BV, Bruns W, Carandini M, Scanziani M. Parvalbumin-expressing interneurons linearly transform cortical responses to visual stimuli. Neuron. 2012; 73:159–170. [PubMed: 22243754]

13. Gentet LJ, et al. Unique functional properties of somatostatin-expressing GABAergic neurons in mouse barrel cortex. Nature Neuroscience. 2012; 15:607–612. [PubMed: 22366760]

14. Lovett-Barron M, et al. Regulation of neuronal input transformations by tunable dendritic inhibition. Nat Neurosci. 2012; 15:423–430. S421–423. [PubMed: 22246433]

15. Murayama M, et al. Dendritic encoding of sensory stimuli controlled by deep cortical interneurons. Nature. 2009; 457:1137–1141. [PubMed: 19151696]

16. Royer S, et al. Control of timing, rate and bursts of hippocampal place cells by dendritic and somatic inhibition. Nat Neurosci. 2012; 15:769–775. [PubMed: 22446878]

17. Kapfer C, Glickfeld LL, Atallah BV, Scanziani M. Supralinear increase of recurrent inhibition during sparse activity in the somatosensory cortex. Nat Neurosci. 2007; 10:743–753. [PubMed: 17515899]

18. Ma Y, Hu H, Berrebi AS, Mathers PH, Agmon A. Distinct subtypes of somatostatin-containing neocortical interneurons revealed in transgenic mice. The Journal of Neuroscience: The Official Journal of the Society for Neuroscience. 2006; 26:5069–5082. [PubMed: 16687498]

19. McGarry LM, et al. Quantitative classification of somatostatin-positive neocortical interneurons identifies three interneuron subtypes. Frontiers in Neural Circuits. 2010; 4:12–12. [PubMed: 20617186]

20. Silberberg G, Markram H. Disynaptic inhibition between neocortical pyramidal cells mediated by Martinotti cells. Neuron. 2007; 53:735–746. [PubMed: 17329212]

21. Hippenmeyer S, et al. A Developmental Switch in the Response of DRG Neurons to ETS Transcription Factor Signaling. PLoS Biol. 2005; 3:e159–e159. [PubMed: 15836427]

22. Taniguchi H, et al. A Resource of Cre Driver Lines for Genetic Targeting of GABAergic Neurons in Cerebral Cortex. Neuron. 2011; 71:995–1013. [PubMed: 21943598]

23. Sohal VS, Zhang F, Yizhar O, Deisseroth K. Parvalbumin neurons and gamma rhythms enhance cortical circuit performance. Nature. 2009; 459:698–702. [PubMed: 19396159]

24. Lima SQ, Hromádka T, Znamenskiy P, Zador AM. PINP: A New Method of Tagging Neuronal Populations for Identification during In Vivo Electrophysiological Recording. PLoS ONE. 2009; 4:e6099–e6099. [PubMed: 19584920]

25. Csicsvari J, Hirase H, Czurko A, Mamiya A, Buzsaki G. Fast network oscillations in the hippocampal CA1 region of the behaving rat. The Journal of Neuroscience: The Official Journal of the Society for Neuroscience. 1999; 19:RC20–RC20. [PubMed: 10436076]

26. Cardin JA, et al. Driving fast-spiking cells induces gamma rhythm and controls sensory responses. Nature. 2009; 459:663–667. [PubMed: 19396156]

27. Fujisawa S, Amarasingham A, Harrison MT, Buzsaki Gr. Behavior-dependent short-term assembly dynamics in the medial prefrontal cortex. Nature Neuroscience. 2008; 11:823–833. [PubMed: 18516033]

28. Xu X, Callaway EM. Laminar specificity of functional input to distinct types of inhibitory cortical neurons. J Neurosci. 2009; 29:70–85. [PubMed: 19129386]

29. Ascoli GA, et al. Petilla terminology: nomenclature of features of GABAergic interneurons of the cerebral cortex. Nature reviews. Neuroscience. 2008; 9:557–568. [PubMed: 18568015]

30. Isomura Y, Harukuni R, Takekawa T, Aizawa H, Fukai T. Microcircuitry coordination of cortical motor information in self-initiation of voluntary movements. Nat Neurosci. 2009; 12:1586–1593. [PubMed: 19898469]

31. Sohal VS, Zhang F, Yizhar O, Deisseroth K. Parvalbumin neurons and gamma rhythms enhance cortical circuit performance. Nature. 2009; 459:698–702. [PubMed: 19396159]

32. Chow BY, et al. High-performance genetically targetable optical neural silencing by light-driven proton pumps. Nature. 2010; 463:98–102. [PubMed: 20054397]

33. Han X, et al. Millisecond-timescale optical control of neural dynamics in the nonhuman primate brain. Neuron. 2009; 62:191–198. [PubMed: 19409264]

34. Harris KD, Hirase H, Leinekugel X, Henze DA, Buzsaki G. Temporal interaction between single spikes and complex spike bursts in hippocampal pyramidal cells. Neuron. 2001; 32:141–149. [PubMed: 11604145]

35. Schmitzer-Torbert N, Jackson J, Henze D, Harris K, Redish AD. Quantitative measures of cluster quality for use in extracellular recordings. Neuroscience. 2005; 131:1–11. [PubMed: 15680687]

36. Cohen JY, Haesler S, Vong L, Lowell BB, Uchida N. Neuron-type-specific signals for reward and punishment in the ventral tegmental area. Nature. 2012; 482:85–88. [PubMed: 22258508]

37. Lima SQ, Hromadka T, Znamenskiy P, Zador AM. PINP: a new method of tagging neuronal populations for identification during in vivo electrophysiological recording. PLoS One. 2009; 4:e6099. [PubMed: 19584920]

38. Endres DM, Schindelin JE. A new metric for probability distributions. Information Theory, IEEE Transactions on. 2003; 49:1858–3718.

39. Brody CD. Correlations without synchrony. Neural Comput. 1999; 11:1537–1551. [PubMed: 10490937]

40. Averbeck BB, Latham PE, Pouget A. Neural correlations, population coding and computation. Nat Rev Neurosci. 2006; 7:358–366. [PubMed: 16760916]

41. Nikolic D, Muresan RC, Feng W, Singer W. Scaled correlation analysis: a better way to compute a cross-correlogram. Eur J Neurosci. 2012; 35:742–762. [PubMed: 22324876]

42. Csicsvari J, Hirase H, Czurko A, Buzsaki G. Reliability and state dependence of pyramidal cell-interneuron synapses in the hippocampus: an ensemble approach in the behaving rat. Neuron. 1998; 21:179–189. [PubMed: 9697862]

43. Marshall L, et al. Hippocampal pyramidal cell-interneuron spike transmission is frequency dependent and responsible for place modulation of interneuron discharge. J Neurosci. 2002; 22:RC197. [PubMed: 11784809]

44. Hangya B, Li Y, Muller RU, Czurko A. Complementary spatial firing in place cell-interneuron pairs. J Physiol. 2010; 588:4165–4175. [PubMed: 20819942]

45. Bartho P, et al. Characterization of neocortical principal cells and interneurons by network interactions and extracellular features. J Neurophysiol. 2004; 92:600–608. [PubMed: 15056678]

46. Fujisawa S, Amarasingham A, Harrison MT, Buzsaki G. Behavior-dependent short-term assembly dynamics in the medial prefrontal cortex. Nat Neurosci. 2008; 11:823–833. [PubMed: 18516033]

47. Tibshirani R, Walther G, Hastie T. Estimating the number of clusters in a data set via the gap statistic. J Roy Stat Soc B. 2001; 63:411–423.

48. Kepecs A, Uchida N, Zariwala H, Mainen Z. Neural correlates, computation and behavioural impact of decision confidence. Nature. 2008; 455:227–258. [PubMed: 18690210]

49. Van De Werd HJ, Rajkowska G, Evers P, Uylings HB. Cytoarchitectonic and chemoarchitectonic characterization of the prefrontal cortical areas in the mouse. Brain Struct Funct. 2010; 214:339–353. [PubMed: 20221886]

50. Zong H, Espinosa JS, Su HH, Muzumdar MD, Luo L. Mosaic analysis with double markers in mice. Cell. 2005; 121:479–492. [PubMed: 15882628]
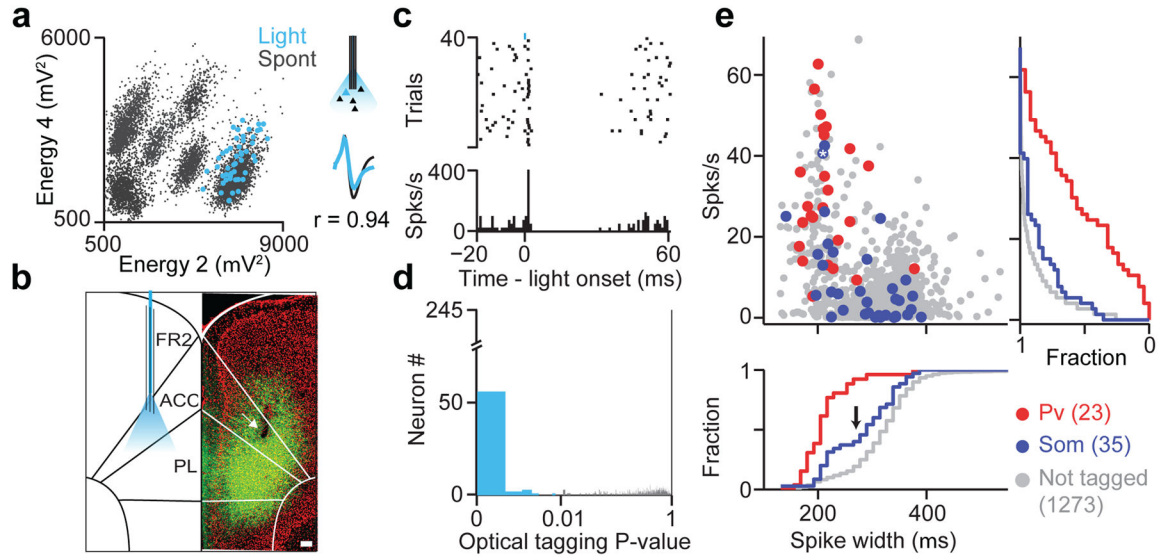
Figure 1. Optogenetic tagging of genetically-defined interneurons in behaving mice
a, Spike sorting example. Unclustered spikes plotted in waveform energy space from two tetrode channels. Light-evoked spikes superimposed in blue, Bottom right, average spontaneous and light-evoked waveforms. **b**, Coronal section from a *Som*-IRES-Cre mouse (green, ChR2; red, DAPI). Arrow indicates electrolytic lesion of recording site in ACC. Scale bar, 100 μm. ACC, anterior cingulate; PL, prelimbic cortex; FR2, frontal region 2. **c**, Spike raster (top) and peri-stimulus time histogram (PSTH) (bottom) for the light-activated cell in **a**, aligned to light onset. Light pulse shown in blue (duration, 1ms; power, ~100mW/mm^2; frequency, 10Hz). **d**, Histogram of SALT (optical tagging test) *P*-values showed strong bimodal distribution; (*P*<0.01, blue). **e**, Firing rate as a function of spike width for *Pv*, *Som* and not tagged neurons. Asterisk indicates neuron in (**a, c**). Cumulative histograms of firing rate (right) and spike width (bottom) are plotted for all groups. Arrow marks mode separation of spike width distribution for *Som* neurons.
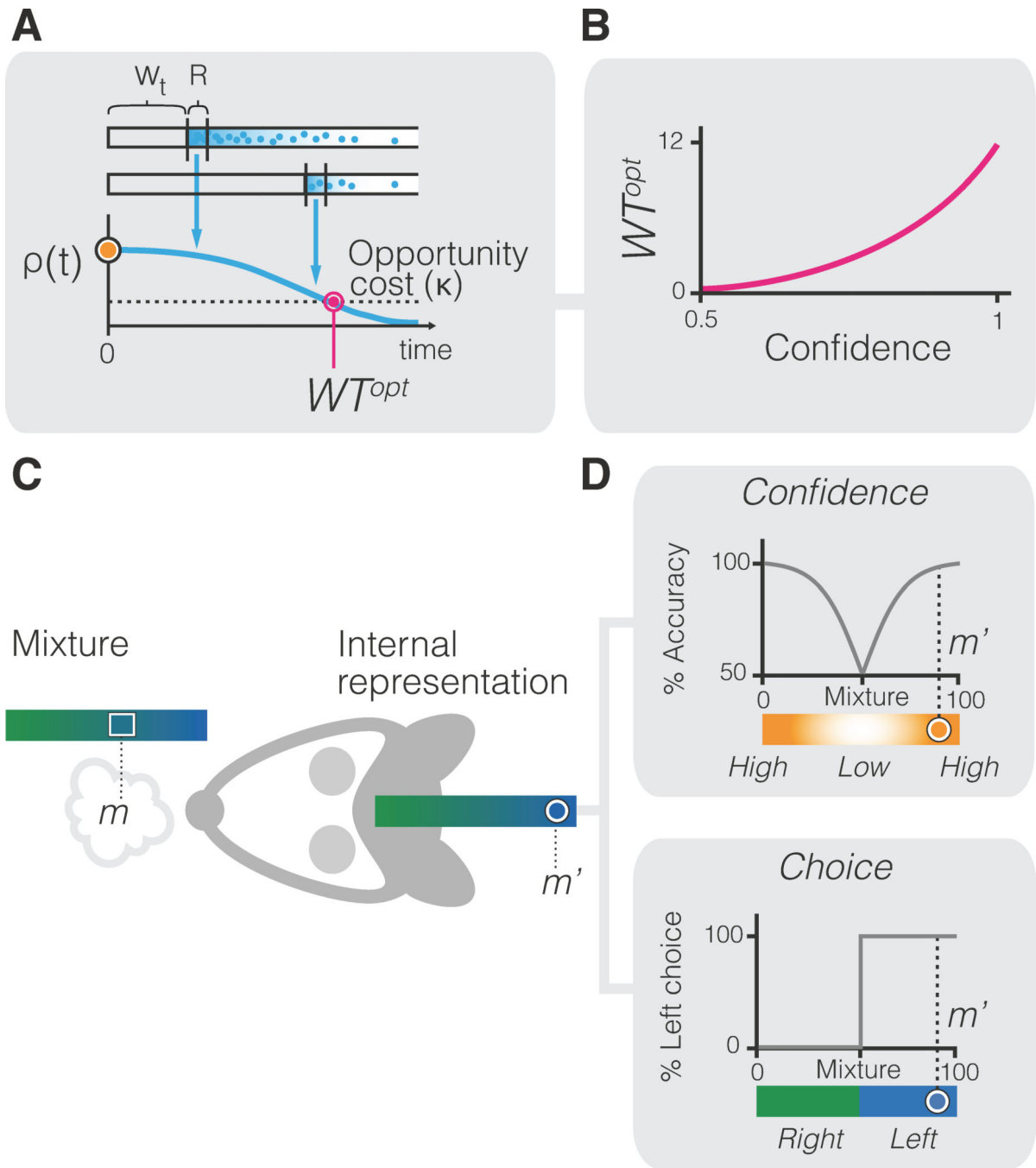
Figure 2. Distinct inhibitory impact of *Som* and *Pv* interneurons
a, b (Top), Spike raster and PSTH of *Pv* (**a**) and *Som* (**b**) interneuron aligned to light onset. (Bottom), PSTH of three simultaneously recorded unidentified neurons. **c**, Average cross-correlograms (CCG) between *Pv-Pv* (top left), *Pv*-Not tagged (bottom left), *Som-Som* (top right), and *Som*-Not tagged (bottom right) neuron pairs; examples of significant pairwise interactions (left Inset) and summary for statistically significant CCG interactions (right inset).
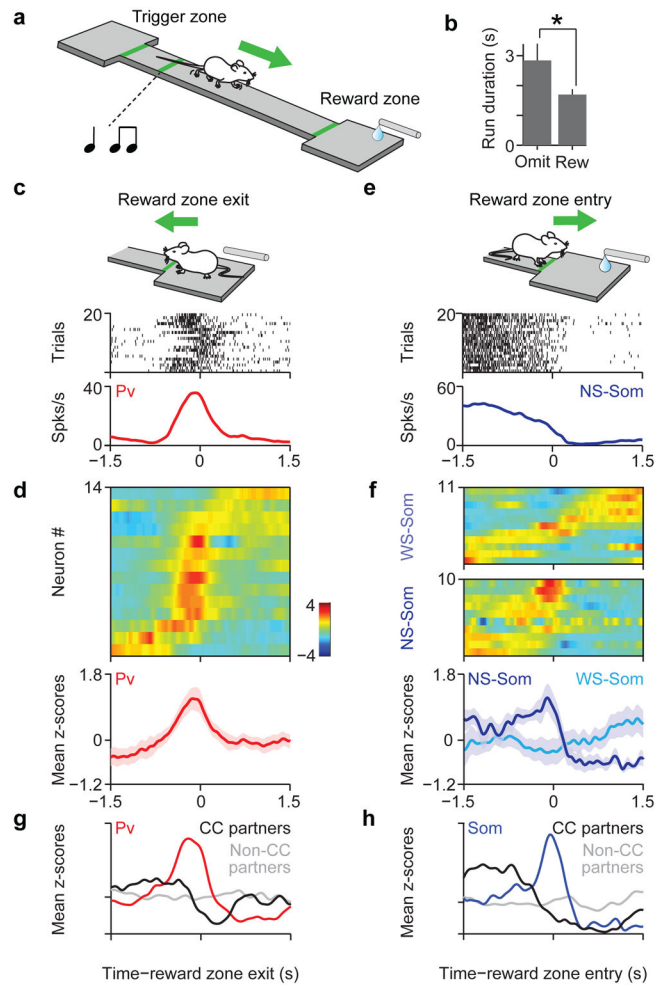
Figure 3. Distinct behavioral correlates of *Pv* and *Som* interneurons

a, Cartoon of mouse performing the reward foraging task **b**, Average run duration for rewarded and omission trials (n = 63 sessions, $P < 0.05$, Mann Whitney U test). **c**, Spike raster and peri-event time histogram (PETH) for an identified *Pv* interneuron aligned to time of reward zone exit. **d**, Top, z-scored PETHs of 14 *Pv* neurons sorted by latency to half-peak firing; bottom, mean z-scored response (shaded area indicates S.E.M.). **e**, Spike raster and PETH for a NS-*Som* interneuron aligned to time of reward zone entry. **f**, Top, z-scored PETHs of 21 *Som* neurons. NS-*Som* and WS-*Som*s are separated. Bottom, mean responses for NS-*Som* and WS-*Som* neurons. **g**, average PETH for *Pv* interneurons (red, *n=4*), with significant inhibitory cross-correlations, (CC-partners, black, *n=5*) and non-CC partners (gray, *n=76*). **h**, Average PETH for *Som* interneurons (blue, *n=3*), CC-partners (black, *n=3*) and non-CC partners (gray, *n=34*)
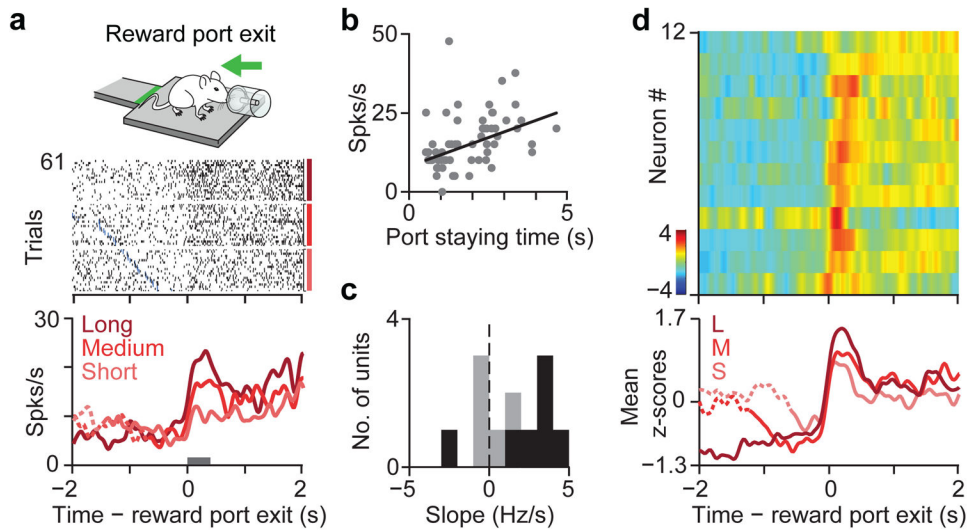
Figure 4. *Pv* interneurons in ACC signal stay duration at foraging decisions
a, Mouse exiting the reward port (inset). Response of a *Pv* neuron during reward port exit. Raster is sorted by staying time in the port and grouped into terciles. Blue ticks denote water valve offset. PETH is shown for each tercile. **b**, Linear regression between firing rate of neuron in (**a**), (epoch indicated by a gray bar) and staying time is significantly positive (r=0.16, slope, 3.63, *P*<0.005). **c**, Histogram of regression slopes for all *Pv* neurons. Black bars indicate significant (*P* < 0.05) regression. **d**, Top, z-scored PETHs of 12 *Pv* neurons aligned to reward-port exit sorted according to latency of half-peak firing. Bottom, average PETH for *Pv* population grouped into staying time terciles.